

## 超快贝塞尔光束在硫化锌晶体表面制备纳米孔

常改艳 王玉恒 程光华

### Writing nanopores on a ZnS crystal with ultrafast Bessel beams

CHANG Gai-yan, WANG Yu-heng, CHENG Guang-hua

引用本文:

常改艳, 王玉恒, 程光华. 超快贝塞尔光束在硫化锌晶体表面制备纳米孔[J]. *中国光学*, 2021, 14(1): 213-225. doi: 10.37188/CO.2020-0101

CHANG Gai-yan, WANG Yu-heng, CHENG Guang-hua. Writing nanopores on a ZnS crystal with ultrafast Bessel beams[J]. *Chinese Optics*, 2021, 14(1): 213-225. doi: 10.37188/CO.2020-0101

在线阅读 View online: <https://doi.org/10.37188/CO.2020-0101>

---

## 您可能感兴趣的其他文章

### Articles you may be interested in

#### 固体激光器与光纤激光器对光子晶体光纤棒耦合的分析与对比

Analysis and comparison of solid-state lasers and fiber lasers on the coupling of rod-type photonic crystal fiber

*中国光学*. 2018, 11(6): 958 <https://doi.org/10.3788/CO.20181106.0958>

#### 高光束质量高斯非稳腔固体激光器研究

Research on the high beam quality of Gaussian unstable resonators in solid state lasers

*中国光学*. 2019, 12(3): 559 <https://doi.org/10.3788/CO.20191203.0559>

#### 高斯涡旋光束在大气湍流传输中的特性研究

Characteristics of Gaussian vortex beam in atmospheric turbulence transmission

*中国光学*. 2017, 10(6): 768 <https://doi.org/10.3788/CO.20171006.0768>

#### CdSe/ZnS量子点下转换膜的红、绿、蓝顶发射有机发光器件

Top-emitting red, green and blue organic light-emitting devices with CdSe/ZnS quantum dots down-conversion films

*中国光学*. 2019, 12(6): 1431 <https://doi.org/10.3788/CO.20191206.1431>

#### 超快激光制备生物医用材料表面功能微结构的现状及研究进展

Surface functional microstructure of biomedical materials prepared by ultrafast laser: a review

*中国光学*. 2019, 12(2): 199 <https://doi.org/10.3788/CO.20191202.0199>

#### 参数可控长距无衍射光束的生成方法研究

Generating method of non-diffracting beam with long-distance propagation and controllable parameters

*中国光学*. 2018, 11(1): 100 <https://doi.org/10.3788/CO.20181101.0100>

## Writing nanopores on a ZnS crystal with ultrafast Bessel beams

CHANG Gai-yan<sup>1,2</sup>, WANG Yu-heng<sup>3</sup>, CHENG Guang-hua<sup>4\*</sup>

(1. *State Key Laboratory of Transient Optics and Photonics, Xi'an Institute of Optics and Precision Mechanics, Chinese Academy of Sciences, Xi'an 710119, China;*

2. *University of Chinese Academy of Sciences, Beijing 100049, China;*

3. *Research Center of Semiconductor Lighting and Information Engineering Technology, South China University of Technology, Guangzhou 510641, China;*

4. *School of Electronics and Information, Center for Optical Imagery Analysis and Learning, Northwestern Polytechnical University, 710072 Xi'an, Shaanxi)*

\* *Corresponding author, E-mail: guanghuacheng@nwpu.edu.cn*

**Abstract:** Zinc sulfide (ZnS) crystal is one of the important materials used to make the wide-spectrum infrared window. The ultrafast laser technology for manufacturing the nanopores with high aspect ratio provides an important approach to fabricate the photonic devices such as mid-infrared waveguide Fourier transform spectrometer etc. In this paper, a 40-times-demagnification ultrafast laser direct-writing system was built with a 4f system and a Gaussian-Bessel beam generated by a quartz axicon and a Yb:KGW laser source that operated at a wavelength of 1 030 nm, a repetition rate of 100 kHz and a pulse width tunable from 223 fs to 20 ps. When the pulse energy was changed from 36  $\mu\text{J}$  to 63  $\mu\text{J}$  and the pulse duration was changed from 12.5 ps to 20 ps, the nanopore structure with a diameter of 80~320 nm was successfully written on the ZnS crystal. The surface morphology, diameter and depth of the nanopores were determined by FIB (Focused Ion Beams) ablation and SEM (Scanning Electron Microscopy) imaging. The influence of laser pulse energy and pulse width on the nanopores was studied. The results show that when the pulse width is 20 ps and the pulse energy is 48  $\mu\text{J}$ , the depth of a nanopore is about 270  $\mu\text{m}$ .

**Key words:** ZnS crystal; high aspect ratio nanopores; photonic devices; Gaussian-Bessel beam

---

收稿日期:2020-06-08; 修订日期:2020-06-22

基金项目:国家重点研发计划(No. 2018YFB1107401); 国家自然科学基金(No. 61775236)资助项目

Supported by National Key Research and Development Program (No. 2018YFB1107401); National Natural Science Foundation of China (No. 61775236)

# 超快贝塞尔光束在硫化锌晶体表面制备纳米孔

常改艳<sup>1,2</sup>, 王玉恒<sup>3</sup>, 程光华<sup>4\*</sup>

(1. 中国科学院 西安光学精密机械研究所 瞬态光学与光子技术国家

重点实验室, 陕西 西安 710119;

2. 中国科学院大学, 北京 100049;

3. 华南理工大学 广东省半导体照明与信息化工程技术研究中心, 广东 广州 510641;

4. 西北工业大学 电子信息学院 光学影像分析与学习中心, 陕西 西安 710072)

**摘要:**硫化锌(ZnS)晶体是重要的宽光谱红外窗口材料, 高深径比纳米孔的超快激光制造技术为中红外波导傅立叶变换光谱仪等光子器件的实现提供了重要的技术途径。本文采用中心波长为 1030 nm、重复频率为 100 kHz、脉冲宽度为 223 fs~20 ps 可调的 Yb: KGW 激光光源, 用石英锥镜产生高斯-贝塞尔光束, 并用 4f 系统构建了 40 倍缩束的超快激光直写系统。在能量为 36~63  $\mu\text{J}$ , 脉宽为 12.5~20 ps 的情况下, 在 ZnS 晶体上成功刻写了直径为 80~320 nm 的纳米孔结构。通过聚焦离子束(FIB)剥蚀和扫描电子显微镜(SEM)成像确定了纳米孔隙表面形貌、直径及深度信息。研究了激光脉冲能量、脉冲宽度对纳米孔隙的影响。结果表明, 在 20 ps 脉冲宽度、48  $\mu\text{J}$  脉冲能量的激光参数下, 纳米孔隙的深度约为 270  $\mu\text{m}$ 。

**关键词:**硫化锌晶体; 高深径比纳米孔; 光子器件; 高斯-贝塞尔光束

中图分类号: TN249

文献标志码: A

doi: 10.37188/CO.2020-0101

## 1 Introduction

The mid-infrared photonics has attracted considerable attention because its wavebands cover thermal imaging bands, multiple atmospheric windows (3~5  $\mu\text{m}$  and 8~14  $\mu\text{m}$ ) necessary for free space communication, as well as main absorption bands of most chemical and biological molecules. It is an inevitable trend for photonic integration to cut costs, improve performance and miniaturize special optical instruments, for example, micro-scale photonic circuits are manufactured in optical materials with a transparent window up to 20  $\mu\text{m}$ . The application of integrated photonics has promoted the rapid development of optical communication technology and the expansion of applied wavelength from near infrared to middle and far infrared. However, the infrared window materials in medium and long wave bands are very limited, mainly including GaAs, GaP, ZnSe, ZnS, InSb, etc.<sup>[1-4]</sup>. Considering the optical and mechanical properties of these materials, ZnS crystal has become one of the most

promising infrared optical materials due to its advantages such as low absorption, high hardness, large Young's modulus, wide transparent window (0.37~14  $\mu\text{m}$ ) and good chemical stability<sup>[5]</sup>. The performance of photonic devices is related to nonlinear optics, the response of materials to the interaction between light and matter, and the balance between the relaxation processes of materials. This means that it is necessary to precisely control the interaction between light and matter and the size of photonic devices so as to realize effective optical transmission and control in complex optical systems.

Ultra-fast Bessel pulse laser is the combination of ultra-fast laser pulse and spatial beam shaping (zero-order Bessel beam) and is formed by symmetric interference between the plane wave and the wave vector distributed on the conic bus. It has a long non-diffraction transmission distance (focal depth  $DOF = W/2 \cdot \tan\theta$ , where  $W$  is the radius of incident Gaussian beam and  $\theta$  is the beam half-cone angle in the Bessel region) and good transmission robustness (self-recovery)<sup>[6-8]</sup>. An ideal Bessel beam

has a narrow and strong central interference region<sup>[9-10]</sup>. This indicates that the Bessel beam is superior to the Gaussian beam in the micro-nano machining of extended micro-channels. For example, the Bessel beam has been used to successfully prepare the nanopore micro-channel structure with an aspect ratio of 10 000:1 in borosilicate glass<sup>[11-13]</sup>. In addition, ultrafast Bessel laser pulses have shown strong applicability in the high-depth and large-area machining, the micro-nano welding, and the development of a mix of micro-nano scale features with new photonic functions<sup>[6,12-14]</sup>. Although ZnS crystal is one of the most promising infrared window materials, its high nonlinear coefficient can cause serious distortion of temporal and spatial distribution of laser pulses when the focused femtosecond laser is transmitted in this crystal. Moreover, the self-focusing and the self-defocusing of plasma can cause spatial beam splitting so that the laser energy cannot be effectively concentrated on the focus. Early experimental and theoretical studies showed that the peak power density could be effectively reduced by pulse broadening, thus weakening the nonlinear effect. 15ps-20ps Ti-sapphire pulsed laser can effectively absorb laser energy and write waveguide in sulfide glass. In the early stage, ultra-fast Bessel beam was used to fabricate the nanopores mainly in quartz glass, silicate glass and borosilicate glass, whose nonlinear absorption was different from that of ZnS by orders of magnitude. Secondly, the hardness, thermal diffusion coefficient and Young's modulus of ZnS crystal are also significantly different from those of the above glass. Therefore, it is difficult to fabricate nanopores on ZnS crystal with ultrafast laser. So far, the preparation of periodic subwavelength microstructures on ZnS crystal has been reported<sup>[15]</sup>. However, the use of ultrafast laser to process the nanopores with high aspect ratio on ZnS crystal is still in blank. In Ref. [16], we reported and discussed the influence of beam mode on the quality of drilling on ZnS crystal. The experimental results show that on ZnS crystal, the pore-forming quality of Bessel beam is better than that of Gaussian beam. Therefore, the use of Bessel laser to directly write

nanoscale microstructures on ZnS crystal, to prepare various medium-infrared optical components and to improve or achieve one of their capabilities has become the current research hotspot of medium-infrared integrated photonics, with a broad application prospect.

In this paper, a Yb:KGW femtosecond laser with the central wavelength of 1 030 nm, the repetition frequency of 100 kHz, and the pulse width of 223 fs was used to generate the Gauss-Bessel beam through an axicon. Then the parameter ranges of the nanopores fabricated on the surface of ZnS crystal were studied. The morphology of nanopores was analyzed by using a Focusing Ion Beam (FIB, Helios G4 CX) and a Scanning Electron Microscope (SEM, JEOL JSM-7500F). The dependence of the surface morphology, diameter and depth of nanopores on laser pulse energy and pulse width was determined. The potential applications of nanopores were discussed.

## 2 Experimental device

The Bessel beam generation device described in Ref. [8], as shown in Fig. 1, is used in this experiment. Firstly, the beam is expanded to 8 mm, and the beam diameter will affect the focusing depth. Applying a combination of an axicon with 1° base angle (Altechna, 1-APX-2-H254-P,  $n = 1.45$ ), focusing lens  $L_1$  with focal length  $f_1 = 400$  mm, and the 20× near-infrared focusing objective lens  $L_2$  with  $f_2 = 10$  mm (Mitutoyo NIR, numerical aperture  $NA = 0.42$ , working distance  $L = 20$  mm), and using a spatial filtering system, we build an experimental device for generating zero-order Bessel beam laser direct-writing microstructure. A Yb:KGW mode-locked regenerative laser amplification system (Pharos, Light Conversion) with a central wavelength of 1 030 nm and adjustable repetition frequency is used to write nano-pore microstructures on ZnS crystal. The pulse width can be continuously adjusted within 223 fs~25 ps by a removable grating compressor in the laser system. The energy of laser pulse is regulated by a half-wave-plate Po-

larized Beam Splitter (PBS). The sample where the nanopores are written is an 18 mm×8 mm×2 mm four-sided polished ZnS crystal. It is fixed to a computer-controlled XYZ 3D high-precision air bearing platform (Aerotech, ANT130). A focusing lens is used to focus the beam on the sample. A high-precision (75 nm) NC system is used to move the sample at a constant speed during the irradiation with a continuous laser pulse. The nanopore spacing can be adjusted by the repetition frequency of the laser source and the translational velocity of the sample ( $A = v/f$ ). During continuous laser irradiation, the Aerotech platform moves the sample at a constant speed (in the positive direction of  $X$ -axis) and simultaneously moves the relative movement with respect to the laser focus (in the negative direction of  $Z$ -axis) to ensure that a new exposure area is always placed in the laser action area. This writing method can help observe the dynamic evolution process of the pore diameter inside the polished sample.

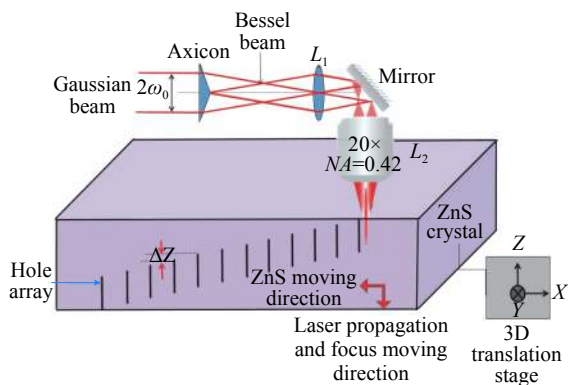


Fig. 1 Experimental setup for microchannel writing with Bessel laser

图 1 贝塞尔激光刻写微通道结构实验装置图

### 3 Experimental results and analysis

The focusing ultrashorter laser pulse has ultra-high peak power and can selectively induce a series of nonlinear effects of transparent materials, such as multi-photon absorption, Kerr effect, plasma self-focusing and self-defocusing, so as to change the microregion morphology and molecular structure of the materials<sup>[17]</sup>. For the ultra-fast laser with a pulse width of 20 ps and a wavelength of 1  $\mu\text{m}$ , its air ionization threshold is approximately  $2.7 \times 10^{13} \text{ W/cm}^2$ <sup>[18]</sup>.

It can be calculated that, in this experiment, the laser power density range acting on ZnS crystal is  $0.57 \times 10^{13} \sim 6.02 \times 10^{13} \text{ W/cm}^2$ . When the laser power density is greater than the ionization threshold of air or ZnS crystal, the laser pulse will generate strong nonlinear absorption in the focus area and cause the formation of plasma, thus effectively absorbing the laser energy and forming a local deposition area with high energy density<sup>[19]</sup>. The extreme high temperature and pressure in the focus area leads to phase transition and micro-explosion, and the energy diffuses from the focus area to the surrounding material in the form of shock wave, so as to construct a 3D micro-nano structure inside the transparent material<sup>[20-22]</sup>. By discussing and analyzing the deposition energy from the nonlinear transmission of laser pulse inside transparent material as well as the possible thermal mechanism, the phase change and the formed microstructural morphology can be controlled more easily. For the laser parameters and air/ZnS crystal interface issue in this experiment, the nonlinear Schrodinger equation in common use can be used to calculate the concentration of plasma in the focus region. However, the mechanism of micro-explosion on the air/crystal interface is more complex. By referring to the parameters and law of femtosecond laser waveguide writing on quartz glass and sulfide glass<sup>[23-24]</sup>, this experiment studied the features of the microstructure fabricated by Bessel beam on ZnS crystal surface when the pulse width changed from femtosecond to 20 ps and the energy changed from damage threshold to 63  $\mu\text{J}$ . The FIB, SEM and phase contrast microscope (PCM, Olympus BX51) were used to characterize the morphology and length of nanopores and microchannels on the sample surface and determine the dependence of surface morphology, diameter and depth of nanopores on laser pulse energy and pulse width.

#### 3.1 Features of nanopores on ZnS crystal surface

Pulse energy and pulse width are the key parameters that affect the interaction between laser and matter. Pulse energy determines the effective radi-

ation flux that the unit area of material is exposed to in unit time. Pulse width is related to the axial energy deposition efficiency of Bessel laser beam<sup>[6,25]</sup>. The experimental and numerical results of the interaction between ultrafast beam and quartz glass and of micro-nano fabrication show that several picoseconds of pulses can effectively overcome the decrease of laser focus plasma density caused by strong nonlinear effects. Considering spatial and temporal focusing characteristics, the nonlinear numerical simulation results of this material show that the plasma concentration generated by the 4.7-ps pulse ionized at the focal point is one order of magnitude higher than that generated by the 60-fs pulse of the same energy<sup>[6]</sup>. However, the nonlinear absorption coefficient of ZnS is one order of magnitude higher than that of common glass, so in the process of pulse width optimization, the range of pulse variation needs to be increased. During the experiment, the maximum pulse width was adjusted to 25 ps by adjusting the compressor of the regenerative amplifier to cover the writing range of the sulfide waveguide<sup>[26]</sup>. When the laser pulse width was increased from 10 ps to 20 ps, the damage threshold range of the ZnS crystal used in this experiment was 6.51~8.32 J/cm<sup>2</sup>. The detailed measurement and calculation methods have been reported in Ref. [27].

The Fig. 2 is a picture of the nanopores on the sample surface, which was obtained from SEM characterization without any post-treatment. During the SEM morphology characterization, the ZnS surface was coated with a gold film about 50 nm thick to become conductive. The black dots at the center of the white ring are nanopores, each of which is written with a single pulse. The white halo around the nanopores is formed by the sputtering or redeposition of the material removed during laser processing. Similar material deposition principles have been reported in Ref. [28]. ZnS crystal is an important wideband infrared window material with strong photosensitivity and inherent sub-stability. Its band gap width is 3.6~3.8 eV. Under the 1030-nm infrared laser radiation, it performs the three-photon absorption. Its nonlinear absorption coefficient ( $a_3 =$

$0.5 \times 10^{-3} \text{ cm}^3/\text{GW}^2$ ) is two orders of magnitude higher than quartz glass. These characteristics indicate the necessity of spatiotemporal envelope control of ultrafast laser pulses<sup>[15]</sup>. Pulse width is a parameter sensitive to ZnS crystal surface damage. The Fig. 2 shows that 12.5-ps pulse width is the critical value where a nanopore will occur. When the pulse width was less than 12.5 ps, the nanopores with a aspect ratio did not appear in the pulse energy range of 35.83~62.82  $\mu\text{J}$ . Instead, the pits with certain depth appeared, as shown in the left column of Fig.2. This is because under short-duration pulses, the carrier generation speed is faster and the plasma defocusing efficiency is higher, so that the axial energy deposition density will be reduced and the thermodynamic conditions for micro-explosion can't be met<sup>[29]</sup>.

The Fig. 3 shows the dependence of nanopore diameter on the pulse width and energy of Bessel beam. The minimum nanopore diameter on ZnS crystal surface was measured by SEM to be 80 nm, and was written by the laser with a pulse width of 12.5 ps and pulse energy of 48.67  $\mu\text{J}$ . The curves in Fig. 3 show that when the pulse energy is fixed, the nanopore diameter will increase with the pulse width within the pulse width window of 12.5~20 ps. When the pulse width is fixed, the nanopore diameter will increase with the pulse energy. Moreover, the greater the energy is, the more obvious this trend will be. However, this does not seem to be the case at the pulse width of 12.5 ps. Since pulse width is a parameter sensitive to crystal surface ablation, the laser near the critical pulse width 12.5 ps can cause various nonlinear effects to interact with each other and result in the instability of nanopore. All the experiments in this paper demonstrate the damage characteristics under monopulse action, which are significantly different from the results of multi-pulse action<sup>[30]</sup>. As far as monopulse is concerned, the self-organizing interference is difficult to occur, and the modulation of laser intensity in the focus area and of plasma intensity is not obvious.

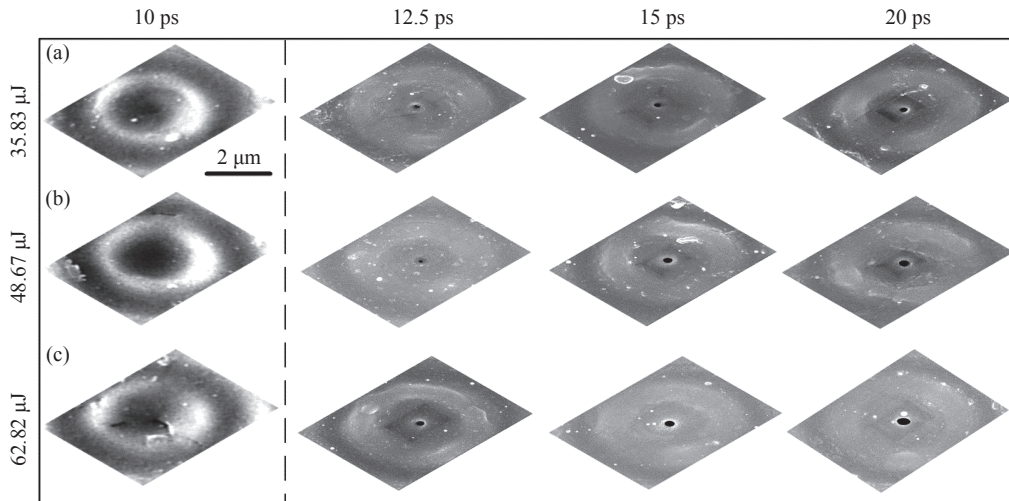


Fig. 2 SEM images of nanopores on ZnS surface at various pulse energies. (a) 35.83  $\mu\text{J}$ ; (b) 48.67  $\mu\text{J}$ ; (c) 62.82  $\mu\text{J}$ . The laser pulse widths in columns 1 to 4 are 10 ps, 12.5 ps, 15 ps and 20 ps respectively

图 2 不同激光参数下 ZnS 表面纳米孔隙结构的 SEM 形貌。(a) 35.83  $\mu\text{J}$ ; (b) 48.67  $\mu\text{J}$ ; (c) 62.82  $\mu\text{J}$ 。第 1 到 4 列的激光脉冲宽度分别是 10ps, 12.5 ps, 15 ps 和 20 ps

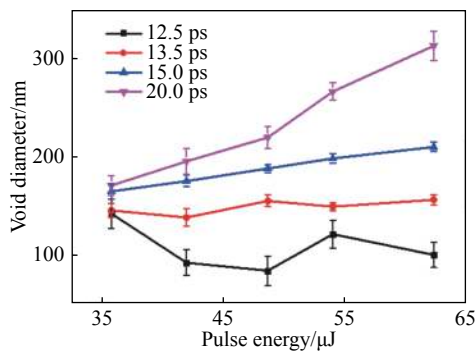


Fig. 3 Nanopore diameter on ZnS crystal surface changes with pulse energy under different laser pulse widths  
图 3 不同激光脉冲宽度下 ZnS 晶体表面纳米孔隙直径随脉冲能量的变化情况

The dynamic process of nanopore formation is generally divided into three stages. The first stage is the nonlinear absorption of crystal and the distortion of pulse space-time. In this stage, different laser parameters directly affect the absorption and deposition of energy in the focus area. The second stage is plasma relaxation, which includes the release of backscattering pressure of high temperature electrons and the transfer of electron energy to the lattice to cause lattice heating and deformation. The third stage is mainly thermal process and lattice relaxation lasting from picoseconds to microseconds. The change of refractive index of quartz glass under the action of ultra-fast Bessel beam can be seen

from time-resolved phase contrast photographs and plasma luminescence intensity. For example, the refractive index of fs time window decreases, that of ps window increases, and those of ns and  $\mu\text{s}$  time windows decrease. However, it is difficult to determine whether the nanopores are formed in the femtosecond stage or nanosecond stage. Both the backscattering pressure of the electrons and the rapid expansion caused by thermal effect may lead to micro-explosion. The self-focusing and self-defocusing effects in nonlinear absorption process and the Rayleigh Taylor instability in fluid dynamics process will lead to the irregular change of nanopore diameter<sup>[19]</sup>.

### 3.2 Features of nanopores in ZnS

AFM, SEM and other surface analysis tools are powerless to characterize the 3D morphology of the nanopores with high depth-diameter ratio. Therefore, in order to obtain the longitudinal morphology features of nanopores, the characterization method of "FIB denudation +SEM imaging" was selected. The FIB etching process enables us to minimize the damage to one-dimensional Bessel pores so that we can analyze the longitudinal morphology of nanopores more intuitively. The results of SEM surface characterization showed that, under 20-ps pulse

width and 62.82- $\mu\text{J}$  pulse energy, the nanopore structure on the surface of ZnS crystal was an oval rather than a regular circle occurring under other laser parameters. Under overhigh peak power density, the Bessel beam was subjected to unexpected nonlinear effects on the crystal surface, which affected the normal transmission of the beam. The possible influencing mechanisms include: Kerr self-focusing, plasma self-defocusing, multi-photon ionization, and plasma shielding. These effects work together to constrain the strength of the Bessel beam on the material surface. Therefore, 20-ps pulse width and 48.67- $\mu\text{J}$  pulse energy are selected as the laser parameters for follow-up study.

The Fig. 4 shows the nanopore structure prepared under 20-ps pulse width and 48.67- $\mu\text{J}$  pulse energy. It can be seen that, the pore channel has a variable diameter along the laser transmission direction. This has something to do with the distribution of axially deposited energy density of Bessel pulse laser during the nonlinear optical transmission inside the material.<sup>[6]</sup> The appearance of pore wall indicates that the material has undergone a process of melting and resolidification. The white flake on the microstructure surface is the residual of the gold film which was applied on the sample surface for conductive use during the SEM characterization and then ultrasonically cleaned. The chemical composition of the white flake was characterized by energy spectrometer (EDS). The results showed that the flake was gold. The lamination diagram along the FIB etching direction is helpful to observe the morphological changes of pore microchannels during the etching process. It can be seen that the pore microchannel transitions from about 3  $\mu\text{m}$  to a larger length as the FIB etching goes on. Because the FIB etching direction can't be easily aligned to the extension direction of the pore, the information on nanopores isn't exhaustive in this paper. To learn more about the pore depth, we observed the side of the nanopore by optical phase contrast microscope.

The Fig. 5(b) shows the side view of pore microchannels under a 20 $\times$  phase contrast microscope

(transmission type). In the PCM transmission-type microscope, the phase shift corresponding to negative refractive index change looks darker on the gray background. For quartz glass, the black traces indicate that the increase in refractive index, while the white traces is the nanopore or gratings with decreasing refractive index. But for sulfide glass with high refractive index, the change of refractive index cannot be judged by diffraction contrast. On the one hand, the refractive index varies greatly and the phase may be inverted; on the other hand, the indication left after laser damage has strong scattering<sup>[25]</sup>. The above enlarged view shows that the microchannels have good uniformity without fault. The nanopore fabricated on ZnS crystal by 20 ps/48.67  $\mu\text{J}$  Bessel laser pulse is about 270  $\mu\text{m}$  long. The refractive index of ZnS crystal is higher than that of quartz glass. If there is no nonlinear effect, the effective length of Bessel beam focus in the ZnS crystal should be larger than that of quartz glass. However, both the simulation and experimental results show that the length of nanopore in ZnS is only half of that in quartz glass. The main reason is that the travel of a nanopore is a highly nonlinear process. It is difficult to derive the law of pore pattern change in the two materials from a single parameter. To explore the positive morphology and pore size change of nanopores inside the material, the sample surface was repeatedly polished, gold-plated and characterized by SEM. The Fig. 5(a) is a SEM image of the cross section of the polished micro-channel. The measurement results show that the pore diameter is about 180 nm, 40 nm smaller than the unpolished diameter. To verify the operability and repeatability of microchannels, several pore microchannels spaced 15  $\mu\text{m}$  apart were processed on the ZnS crystal by using the Bessel beams with the same pulse width and energy (20 ps, 48.67  $\mu\text{J}$ ). Three of them are shown in 5(b). From Fig. 4 and Fig. 5, the accurate information on nanopore depth cannot be obtained, except for the information of 3  $\mu\text{m}$  < pore depth < 270  $\mu\text{m}$ , which is about half of the pore depth on the



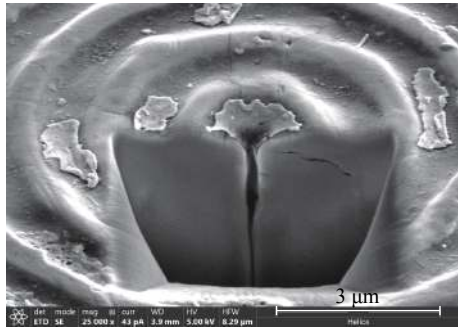


Fig. 4 SEM image of cross section of FIB-etched nanopore

图 4 FIB 刻蚀纳米孔隙横截面处的 SEM 形貌图

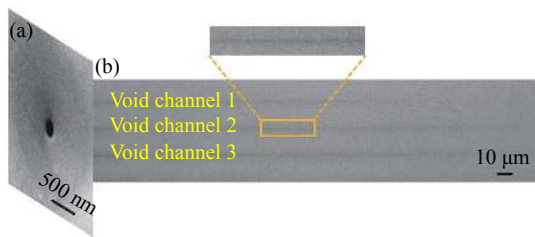


Fig. 5 Characteristics of nanopore inside ZnS crystal. (a) SEM image of cross-section of polished nanopore; (b) side view of the nanopore under a  $20\times$  phase contrast microscope (transmission microscopy type). The upper inset is an enlarged view of a microchannel. Note that all the microstructures in the picture are written under the laser parameters of 20 ps and 48.67  $\mu\text{J}$

图 5 ZnS 晶体内部纳米孔隙的结构特征。(a) 抛光后纳米孔隙横截面的 SEM 图; (b)  $20\times$  相衬显微镜下的纳米孔隙结构的侧面图 (透射式显微模式), 上方插图是微通道的放大图, 图中的微结构均是在 20 ps, 48.67  $\mu\text{J}$  的激光参数下刻写的

——中文对照版——

## 1 引言

中红外光子学因其波段覆盖了热成像、自由空间通信所必需的多个大气窗口 ( $3\sim 5\ \mu\text{m}$  和  $8\sim 14\ \mu\text{m}$ ), 以及大多数化学和生物分子的主要吸收带, 而引起了广泛关注。光子集成以降低成本、提高性能为目标, 专用光学仪器小型化是必然趋势, 例如在透明窗口高达  $20\ \mu\text{m}$  的光学材料中制造微尺度光子电路。集成光子学的应用促进了光通信技术的快速发展, 应用波长也由近红外

surface of optimized quartz glass. Even so, it is still of great significance to fabricate nanopores in mid-infrared sulfide glass and sulfide crystal. This technique has laid an important technical foundation for the realization of mid-infrared waveguide/standing-wave waveguide Fourier transform spectrometer<sup>[31-32]</sup>. Its applications in mid-infrared photonic crystals, mid-infrared microfluidic devices and photonic screens are of great significance<sup>[33]</sup>.

## 4 Conclusion

The nanopore structures with high aspect ratio were written in ZnS crystal with ultrafast Bessel laser. By adjusting the laser parameters, the optimal energy window ( $36\sim 63\ \mu\text{J}$ ) and pulse width window ( $12.5\sim 20\ \text{ps}$ ) for nanopore writing on ZnS crystal were obtained to fabricate the nanopores with a diameter of  $80\sim 320\ \text{nm}$ . By using the scanning electron microscope, focused ion beam and phase contrast microscope, the morphology and length of nanopores and pore channels on the sample surface were characterized, and the dependence of surface morphology, diameter and depth of nanopores on laser pulse energy and pulse width was identified. This technique is of great significance to the fabrication of mid-infrared waveguide Fourier transform spectrometer and sulfide photonic crystal.

向中、远红外扩展。但是, 中长波红外窗口材料十分有限, 主要有 GaAs, GaP, ZnSe, ZnS, InSb 等<sup>[1-4]</sup>。综合考虑材料的光学特性和机械性能, ZnS 晶体以其低吸收, 高硬度, 大的杨氏模量和透明窗口 ( $0.37\sim 14\ \mu\text{m}$ ) 以及良好的化学稳定性等优势成为最具应用前景的红外光学材料之一<sup>[5]</sup>。光子器件的性能与非线性光学材料对光与物质相互作用的响应以及材料弛豫过程之间的平衡有关。这意味着必须精确控制光与物质相互作用的过程及光子器件尺寸, 以在复杂的光学系统中有效进行光传输和控制。

超快贝塞尔脉冲激光将超快激光脉冲和光束空间整形(零阶贝塞尔光束)相结合,由平面波与分布在圆锥母线上的波矢量对称干涉形成,其无衍射传输距离(焦深  $\text{DOF} = W/2 \cdot \tan\theta$ ,  $W$  是入射高斯光束半径,  $\theta$  是贝塞尔区的光束半锥角)长,传输鲁棒性(自恢复)好<sup>[6-8]</sup>。理想的贝塞尔光束具有窄而强的中心干涉区域<sup>[9-10]</sup>。这表明在扩展微通道长度微纳加工方面,贝塞尔光束优于高斯光束,如贝塞尔光束在硼硅酸盐玻璃中成功制备了深径比为 10000:1 的纳米孔微通道结构<sup>[11-13]</sup>。同时,超快贝塞尔激光脉冲在高深度和大面积加工、微纳焊接及开发具有新的光子功能的微纳尺度特征方面显示了强大的适用性<sup>[6,12-14]</sup>。ZnS 晶体是最具前景的红外窗口材料之一,由于其非线性系数高,聚焦后的飞秒激光在硫化锌晶体中传输时,激光脉冲的时间和空间分布会发生严重畸变,自聚焦和等离子体产生的自散焦导致光束空间分裂,激光能量不能有效集中在焦点。前期的实验和理论研究表明,通过脉冲展宽的方法,能有效降低峰值功率密度,从而降低非线性效应,15 ps~20 ps 钛宝石脉冲激光能够在硫化物玻璃内实现激光能量的有效吸收和波导刻写。用超快贝塞尔光束制造纳米孔的工作,前期主要集中在石英玻璃、硅酸盐玻璃以及硼硅酸盐玻璃,其非线性吸收与硫化锌有数量级的差别;其次,硫化锌晶体的硬度、热扩散系数、杨氏模量与上述玻璃也有明显差别。因此,用超快激光在硫化锌晶体上制作纳米孔具有一定难度。到目前为止,在 ZnS 晶体上制备周期性的亚波长微结构的研究虽有报道<sup>[15]</sup>,然而,利用超快激光在 ZnS 晶体上加工高深径比的纳米孔仍处于空白。文献 [16] 报道了光束模式对 ZnS 晶体打孔质量的影响,并进行了讨论。实验结果显示,用贝塞尔光束在 ZnS 晶体上打孔,其成孔质量优于高斯光束。因此,利用贝塞尔激光在 ZnS 晶体上直写纳米级微结构,制备各种中红外光学元器件,提高或实现其某种性能已成为当下中红外集成光子学的研究热点,并且具有广阔的应用前景。

本文使用中心波长为 1030 nm、重复频率为 100 kHz、脉冲宽度为 223 fs 的 Yb:KGW 飞秒激光,用锥镜产生高斯-贝塞尔光束,研究了在 ZnS 晶体表面制造纳米孔的参数范围,用聚焦离子束

(FIB, Helios G4 CX) 剥蚀和扫描电子显微镜 (SEM, JEOL JSM-7500F) 分析了纳米孔隙的形貌,确定了纳米孔隙表面形貌、直径及深度与激光脉冲能量、脉冲宽度的关系,讨论了纳米孔的潜在应用。

## 2 实验装置

实验采用文献 [8] 中的贝塞尔光束生成装置,如图 1 所示。首先将光束扩束到 8 mm,光束直径将影响聚焦深度,采用  $1^\circ$  底角轴棱锥 (Altechna, 1-APX-2-H254-P,  $n=1.45$ ),焦距  $f_1=400$  mm 的聚焦透镜  $L_1, f_2=10$  mm 的  $20\times$  近红外聚焦显微物镜  $L_2$  (Mitutoyo NIR, 数值孔径  $NA=0.42$ , 工作距离  $L=20$  mm) 的组合,利用空间滤波系统产生零阶贝塞尔光束激光直写微结构的实验装置。采用中心波长为 1030 nm、重复频率可调的掺镱钨酸钪钾 (Yb:KGW) 锁模激光再生放大系统 (Pharos, Light conversion) 在 ZnS 晶体上刻写纳米孔隙微结构。通过激光系统中的可移动光栅压缩器可以使脉冲宽度在 223 fs~25 ps 间连续调节。利用二分之一波片偏振分光棱镜 (PBS) 来调节激光脉冲能量。用于刻写纳米孔隙的样品是尺寸为  $18\text{ mm}\times 8\text{ mm}\times 2\text{ mm}$  的四面抛光的硫化锌晶体,将其固定在计算机控制的 XYZ 三维高精空气轴承平台 (Aerotech, ANT130) 上,使用聚焦物镜将光束聚焦到样品上。利用高精度 (75 nm) 数控系统在连续激光脉冲的照射过程中以恒定速度移动样品。纳米孔隙间隔可以通过激光光源的重复频率和样品的平移速度来调节 ( $\Delta = v/f$ )。连续激光辐照过程中, Aerotech 平台以恒定速度同时移动样品 (沿  $x$  轴的正方向移动) 和激光焦点 (沿  $z$  轴的负方向移动),使它们做相对运动,以确保在连续激光辐照过程中,样品始终有一个新的曝光区置于激光作用区内。这种刻写方式,有利于观测抛光后样品内部孔隙直径的动态演变过程。

## 3 实验结果及分析

聚焦的超短激光脉冲具有超高峰值功率,可以空间选择性地诱导透明材料产生一系列非线性效应,如多光子吸收、克尔效应、等离子体自聚焦自散焦等,进而实现材料微区形貌、分子结构等

的改变<sup>[17]</sup>。对于 20 ps 脉冲宽度, 1  $\mu\text{m}$  波长的超快激光, 空气电离阈值约为  $2.7 \times 10^{13} \text{ W/cm}^2$ <sup>[18]</sup>。计算可得, 本实验中作用在 ZnS 晶体上的激光功率密度为  $0.57 \times 10^{13} \sim 6.02 \times 10^{13} \text{ W/cm}^2$ 。当激光功率密度大于空气或硫化锌晶体的电离阈值时, 激光脉冲将在焦点区域产生强烈的非线性吸收, 并形成等离子体, 从而有效吸收激光能量, 形成局部高密度沉积区域<sup>[19]</sup>。焦点区域内形成极端的高温高压条件会导致产生相变和微爆, 并且能量以冲击波的形式自焦点区域向周围材料扩散, 从而在透明材料内部构建微米尺度的三维结构<sup>[20-22]</sup>。对透明材料内部的激光脉冲非线性传输的沉积能量和可能的热机制进行讨论分析, 有利于控制相变和产生的微结构形态。针对本实验中的激光参数和空气/硫化锌晶体界面问题, 常用的非线性薛定谔方程可以用来计算焦点区域内的等离子体浓度。但在空气/晶体界面, 微爆的产生机理更复杂。参考石英玻璃和硫化物玻璃的飞秒激光波导刻写参数规律<sup>[23-24]</sup>, 实验研究了脉冲宽度从飞秒到 20 ps、能量从损伤阈值到 63  $\mu\text{J}$  变化范围内贝塞尔光在硫化锌晶体表面制造微结构的特征, 利用 FIB、SEM 和相衬对比显微镜 (PCM, Olympus BX51) 表征样品表面纳米孔及孔隙通道的形貌和长度信息, 确定了纳米孔隙表面形貌、直径及深度与激光脉冲能量、脉冲宽度的关系。

### 3.1 硫化锌晶体表面纳米孔隙特征

脉冲能量和脉冲宽度是影响激光与物质相互作用的关键参数, 脉冲能量影响材料在单位时间内单位面积所经历的有效辐照通量。脉冲宽度与贝塞尔激光束轴向能量沉积效率有关<sup>[6,25]</sup>。超快光束与石英玻璃相互作用及微纳制造的实验与数值分析结果显示: 几个皮秒的脉冲能够有效克服过强的非线性效应导致的激光焦点等离子体密度下降。考虑时空聚焦特性和材料的非线性数值模拟结果表明, 4.7 ps 的脉冲比 60 fs 相同能量的脉冲在焦点处电离产生的等离子体浓度高一个数量级<sup>[6]</sup>, 然而硫化锌的非线性吸收系数比常见的玻璃高一个数量级。因此在脉冲宽度优化过程中, 需要增加脉冲变化范围。实验过程中, 通过调节再生放大器的压缩器, 将脉冲宽度最大调节到 25 ps, 覆盖了硫化物波导写入范围<sup>[26]</sup>。当激光脉冲宽度由 10 ps 增加至 20 ps 的过程中, 测量得到本实验中使用的 ZnS 晶体的损伤阈值范围为 6.51~

8.32  $\text{J/cm}^2$ , 详细的测量及计算方法见文献 [27]。

在没有任何后处理的情况下, 通过 SEM 表征得到的样品表面纳米孔如图 2 所示。在 SEM 形貌表征时, ZnS 表面被镀约 50 nm 厚的金膜, 以使样品导电。白色圆环中心的黑点就是纳米孔, 每个孔都是由单发脉冲刻写的, 纳米孔周围的白色光晕是激光加工过程中去除的材料溅射或者再沉积而产生的, 类似的材料沉积原理见文献 [28]。硫化锌晶体具有很强的光敏性和固有的亚稳定性, 是重要的宽带红外窗口材料, 禁带宽度为 3.6~3.8 eV, 在 1030 nm 红外激光作用下, 其是三光子吸收, 非线性吸收系数 ( $a_3 = 0.5 \times 10^{-3} \text{ cm}^3/\text{GW}^2$ ) 比石英玻璃高两个数量级。这些特征表明了对超快激光脉冲时空包络控制的必要性<sup>[15]</sup>。脉冲宽度是 ZnS 晶体表面损伤的敏感参数, 图 2 表明 12.5 ps 脉宽是纳米孔隙出现的临界脉宽值, 当脉宽小于 12.5 ps 时, 35.83 ~ 62.82  $\mu\text{J}$  的脉冲能量并未出现具有深径比的纳米孔结构, 而是如图(1)左侧第一列中出现的具有一定深度的凹坑状结构。这是因为在短的脉冲宽度下, 载流子生成速度较快, 等离子体散焦效率相对较高, 使得轴向能量沉积密度减少, 不满足微爆产生的热力学条件<sup>[29]</sup>。

图 3 显示了贝塞尔光束的脉冲宽度及脉冲能量对 ZnS 晶体表面纳米孔直径的影响。用 SEM 测得 ZnS 晶体表面纳米孔隙的直径最小可达 80 nm, 是在脉冲宽度为 12.5 ps, 脉冲能量为 48.67  $\mu\text{J}$  的激光加工参数下刻写的。图中的曲线表明: 固定脉冲能量, 在 12.5 ps ~ 20 ps 的脉宽窗口内, 纳米孔直径随着脉冲宽度的增加而增加; 固定脉宽, 纳米孔直径随着脉冲能量增加而增加, 且能量越大, 这种变化趋势越明显。但在 12.5 ps 时, 不符合这一规律。这是由于脉冲宽度是晶体表面烧蚀的敏感参数, 12.5 ps 为临界脉宽, 激光作用在晶体表面, 产生的各种非线性效应相互影响, 导致孔径变化不稳定。本文所有实验均是单脉冲作用下的损伤特性, 与多脉冲结果具有明显差别<sup>[30]</sup>, 对单脉冲而言, 自组织干涉难以发生, 焦点区域激光强度的调制和等离子体强度的调制不明显。

纳米孔形成的动力学过程一般分为 3 个阶段: 首先是晶体的非线性吸收与脉冲时空的畸变, 不同激光参数直接影响焦点区域能量的吸收与沉积; 其次是等离子体弛豫阶段, 包括高温电子的背

向散射压力的释放,电子能量传递到格子,导致晶格的升温和形变;第三阶段主要是热过程和晶格的弛豫过程,从皮秒持续到微秒。从时间分辨的相位对比照片与等离子体发光强度可以看出石英玻璃在超快贝塞尔光束作用下的折射率改变:fs 时间窗口的折射率降低、ps 窗口的折射率升高,以及 ns 和  $\mu\text{s}$  时间窗口的折射率降低。然而难以判断纳米孔的形成是在飞秒阶段还是纳秒阶段,电子背向散射压力和热效应产生的快速膨胀均可能导致微爆的产生。非线性吸收过程中的自聚焦自散焦效应、流体动力学过程的瑞利泰勒不稳定性都会导致孔径变化的不规律<sup>[19]</sup>。

### 3.2 硫化锌内部纳米孔隙特征

AFM、SEM 等表面分析工具无法表征高深径比纳米孔三维形貌,因此,为了获取纳米孔隙纵向形貌特征,本文选择 FIB 剥蚀+SEM 成像的表征方式。FIB 刻蚀工艺能够将对一维贝塞尔孔隙的损害降到最低,有利于更直观地分析纳米孔的纵向形貌。SEM 表面表征结果显示,在 20 ps 脉冲宽度,62.82  $\mu\text{J}$  脉冲能量的激光参数下,ZnS 晶体表面的纳米孔隙结构是椭圆形,而非像其他激光参数下出现的规则圆形。分析认为在过高的峰值功率密度下,贝塞尔光束在晶体表面经历了非线性效应,影响了光束的正常传输。可能的影响机理:克尔自聚焦、等离子体自散焦、多光子电离、等离子体屏蔽效应。这些效应共同作用,导致贝塞尔光束在材料表面的强度受到钳制。因此,选定 20 ps 脉冲宽度,48.67  $\mu\text{J}$  脉冲能量的激光参数用于后续研究。

图 4 是在 20 ps 脉冲宽度、48.67  $\mu\text{J}$  脉冲能量下制备的纳米孔隙结构。由图 4 可见,该孔隙通道沿着激光传输方向具有可变的直径,这与贝塞尔脉冲激光在材料内部的非线性光传输过程中的轴向沉积能量密度分布有关<sup>[6]</sup>。孔壁表明材料经历了熔化和再凝固的过程。微结构表面的白色片状物是 SEM 表征样品时为了样品导电喷在表面的金膜经过超声清洁后的残留。利用能谱仪(EDS)对该白色片状物进行了化学成分的表征,显示结果为金元素。沿 FIB 刻蚀方向的层叠图有利于观察刻蚀过程中孔隙微通道的形态变化。可以看出,随着 FIB 刻蚀,孔隙微通道从大约 3  $\mu\text{m}$  向更长过渡。由于 FIB 刻蚀方向很难与孔的延伸方向平行,因此,本文中未能获得纳米孔的全部信

息。为了获得更多的孔深信息,用光学相位对比显微镜观察了纳米孔的侧面。

图 5(b) 显示了 20 $\times$  相衬对比显微镜下孔隙微通道的侧面(透射式显微模式)图像。PCM 透射式显微模式中,负的折射率变化对应的相移在灰色背景上显得较暗,对石英玻璃而言,黑色痕迹表示折射率增加,白色表示折射率降低的纳米孔或者纳米光栅。但高折射率的硫化物玻璃则不同。利用衍射衬度无法判断折射率的变化情况:一方面折射率变化大,相位可能倒装;另一方面激光损伤后的痕迹有强散射<sup>[25]</sup>。上方放大图像显示,微通道未出现断层,具有良好的均匀性,用 20 ps、48.67  $\mu\text{J}$  的贝塞尔激光脉冲在硫化锌晶体上制造的纳米孔长度约为 270  $\mu\text{m}$ 。硫化锌晶体的折射率大于石英玻璃,如果没有非线性效应,贝塞尔光束焦点的有效长度在硫化锌晶体内应该大于石英玻璃,然而模拟和实验结果均显示,硫化锌内孔长度只有石英玻璃的一半。这主要因为纳米孔行程是一个高度非线性的过程,难以从单一参数得到两种材料孔型的变化规律。为了探究材料内部纳米孔的正向形貌及孔径变化特征,对样品表面进行反复抛光,镀金以及采用 SEM 表征。图 5(a) 是抛光后微通道横截面的 SEM 图像,测量结果显示孔隙的直径约为 180 nm。与抛光前的直径相比,减小了 40 nm。为了验证微通道的可操作性和可重复性,采用同一脉宽和能量(20 ps、48.67  $\mu\text{J}$ ) 的贝塞尔光束在硫化锌晶体上加工了间隔为 15  $\mu\text{m}$  的多个孔隙微通道,图 5(b) 是截取的其中 3 个微通道。从图 4 和图 5 不能获得纳米孔深度的准确信息,只能判断孔深范围大于 3  $\mu\text{m}$ ,小于 270  $\mu\text{m}$ ,是优化后石英玻璃表面孔深的一半左右。即便如此,在中红外硫系玻璃和硫系晶体中制造纳米孔仍然具有重要意义,为中红外波导驻波波导傅立叶变换光谱仪的实现奠定了重要的技术基础<sup>[31-32]</sup>。对于中红外光子晶体、中红外微流器件、光子筛等应用均有重要意义<sup>[33]</sup>。

## 4 结 论

利用超快贝塞尔激光在 ZnS 晶体中刻写了高深径比的纳米尺度的孔隙结构,通过调控激光参数制造了直径为 80~320 nm 的纳米孔,获得了

在 ZnS 晶体上刻写纳米孔的最佳能量 (36  $\mu\text{J}$  ~ 63  $\mu\text{J}$ ) 及脉宽 (12.5 ps ~ 20 ps) 窗口。利用扫描电子显微镜、聚焦离子束和相衬对比显微镜表征了样品表面纳米孔及孔隙通道的形貌和长度信息,

确定了纳米孔隙表面形貌、直径及深度对激光脉冲能量、脉冲宽度的影响。该技术对中红外波导傅立叶变换光谱仪、硫化物光子晶体制作具有重要意义。

#### 参考文献:

- [1] LIN H T, LUO ZH Q, GU T, *et al.*. Mid-infrared integrated photonics on silicon: a perspective[J]. *Nanophotonics*, 2018, 7(2): 393-420.
- [2] AN Q, REN Y Y, JIA Y CH, *et al.*. Mid-infrared waveguides in zinc sulfide crystal[J]. *Optical Materials Express*, 2013, 3(4): 466-471.
- [3] HU J J, MEYER J, RICHARDSON K, *et al.*. Feature issue introduction: mid-IR photonic materials[J]. *Optical Materials Express*, 2013, 3(9): 1571-1575.
- [4] PILE D, HORIUCHI N, WON R, *et al.*. Extending opportunities[J]. *Nature Photonics*, 2012, 6(7): 407.
- [5] FU L G, LÜ F X, WANG X W, *et al.*. Defects in CVDZnS[J]. *Rare Metals*, 2011, 30(4): 387-391.
- [6] BHUYAN M K, VELPULA P K, COLOMBIER J P, *et al.*. Single-shot high aspect ratio bulk nanostructuring of fused silica using chirp-controlled ultrafast laser Bessel beams[J]. *Applied Physics Letters*, 2014, 104(2): 021107.
- [7] ROSEN J, YARIV A. Synthesis of an arbitrary axial field profile by computer-generated holograms[J]. *Optics Letters*, 1994, 19(11): 843-845.
- [8] STOIAN R, BHUYAN M K, ZHANG G D, *et al.*. Ultrafast Bessel beams: advanced tools for laser materials processing[J]. *Advanced Optical Technologies*, 2018, 7(3): 165-174.
- [9] BHUYAN M K, COURVOISIER F, LACOURT P A, *et al.*. High aspect ratio nanochannel machining using single shot femtosecond Bessel beams[J]. *Applied Physics Letters*, 2010, 97(8): 081102.
- [10] BHUYAN M K, COURVOISIER F, PHING H S, *et al.*. Laser micro- and nanostructuring using femtosecond Bessel beams[J]. *The European Physical Journal Special Topics*, 2011, 199(1): 101-110.
- [11] MITRA S, CHANAL M, CLADY R, *et al.*. Millijoule femtosecond micro-Bessel beams for ultra-high aspect ratio machining[J]. *Applied Optics*, 2015, 54(24): 7358-7365.
- [12] ZHANG G D, STOIAN R, CHENG G H, *et al.*. Femtosecond laser Bessel beam welding of transparent to non-transparent materials with large focal-position tolerant zone[J]. *Optics Express*, 2018, 26(2): 917-926.
- [13] MEYER R, FROEHLI L, GIUST R, *et al.*. Extremely high-aspect-ratio ultrafast Bessel beam generation and stealth dicing of multi-millimeter thick glass[J]. *Applied Physics Letters*, 2019, 114(20): 201105.
- [14] RAPP L, MEYER R, GIUST R, *et al.*. High aspect ratio micro-explosions in the bulk of sapphire generated by femtosecond Bessel beams[J]. *Scientific Reports*, 2016, 6: 34286.
- [15] ZHANG F, DUAN J A, ZHOU X F, *et al.*. Broadband and wide-angle antireflective subwavelength microstructures on zinc sulfide fabricated by femtosecond laser parallel multi-beam[J]. *Optics Express*, 2018, 26(26): 34016-34030.
- [16] LI Y P, ZHANG T H, FAN S L, *et al.*. Fabrication of micro hole array on the surface of CVD ZnS by scanning ultrafast pulse laser for antireflection[J]. *Optical Materials*, 2017, 66: 356-360.
- [17] RUDENKO A, COLOMBIER J P, ITINA T E. Nanopore-mediated ultrashort laser-induced formation and erasure of volume nanogratings in glass[J]. *Physical Chemistry Chemical Physics*, 2018, 20(8): 5887-5899.
- [18] 王晓雷, 张楠, 赵友博, 等. 飞秒激光激发空气电离的阈值研究[J]. *物理学报*, 2008, 57(1): 354-357.  
WANG X L, ZHANG N, ZHAO Y B, *et al.*. Determination of air ionization threshold with femtosecond laser pulses[J]. *Acta Physica Sinica*, 2008, 57(1): 354-357. (in Chinese)
- [19] STOIAN R, BHUYAN M K, RUDENKO A, *et al.*. High-resolution material structuring using ultrafast laser non-diffractive beams[J]. *Advances in Physics: X*, 2019, 4(1): 1659180.
- [20] GLEZER E N, MAZUR E. Ultrafast-laser driven micro-explosions in transparent materials[J]. *Applied Physics Letters*, 1997, 71(7): 882-884.
- [21] JUODKAZIS S, NISHIMURA K, TANAKA S, *et al.*. Laser-induced microexplosion confined in the bulk of a sapphire crystal: evidence of multimegabar pressures[J]. *Physical Review Letters*, 2006, 96(16): 166101.
- [22] GAMALY E G, JUODKAZIS S, NISHIMURA K, *et al.*. Laser-matter interaction in the bulk of a transparent solid:

- confined microexplosion and void formation[J]. *Physical Review B*, 2006, 73(21): 214101.
- [23] ZHANG G D, CHENG G H, BHUYAN M K, *et al.*. Ultrashort Bessel beam photoinscription of Bragg grating waveguides and their application as temperature sensors[J]. *Photonics Research*, 2019, 7(7): 806-814.
- [24] ZHANG G D, CHENG G H, BHUYAN M, *et al.*. Efficient point-by-point Bragg gratings fabricated in embedded laser-written silica waveguides using ultrafast Bessel beams[J]. *Optics Letters*, 2018, 43(9): 2161-2164.
- [25] POLESANA P, FRANCO M, COUAIRO A, *et al.*. Filamentation in Kerr media from pulsed Bessel beams[J]. *Physical Review A*, 2008, 77(4): 043814.
- [26] D'AMICO C, CHENG G H, MAUCLAIR C, *et al.*. Large-mode-area infrared guiding in ultrafast laser written waveguides in Sulfur-based chalcogenide glasses[J]. *Optics Express*, 2014, 22(11): 13091-13101.
- [27] DAM B, RECTOR J, CHANG M F, *et al.*. Laser ablation threshold of  $\text{YBa}_2\text{Cu}_3\text{O}_{6+x}$ [J]. *Applied Physics Letters*, 1994, 65(12): 1581-1583.
- [28] JOGLEKAR A P, LIU H H, MEYHÖFER G, *et al.*. Optics at critical intensity: applications to nanomorphing[J]. *Proceedings of the National Academy of Sciences of the United States of America*, 2004, 101(16): 5856-5861.
- [29] GAMALY E G, VAILIONIS A, MIZEIKIS V, *et al.*. Warm dense matter at the bench-top: Fs-laser-induced confined micro-explosion[J]. *High Energy Density Physics*, 2012, 8(1): 13-17.
- [30] CHENG G H, RUDENKO A, D'AMICO C, *et al.*. Embedded nanogratings in bulk fused silica under non-diffractive Bessel ultrafast laser irradiation[J]. *Applied Physics Letters*, 2017, 110(26): 261901.
- [31] MARTIN G, BHUYAN M, TROLES J, *et al.*. Near infrared spectro-interferometer using femtosecond laser written GLS embedded waveguides and nano-scatterers[J]. *Optics Express*, 2017, 25(7): 8386-8397.
- [32] DOUGLASS G, ARRIOLA A, HERAS I, *et al.*. Novel concept for visible and near infrared spectro-interferometry: laser-written layered arrayed waveguide gratings[J]. *Optics Express*, 2018, 26(14): 18470-18479.
- [33] SHANKAR R, LEIJSEN R, BULU I, *et al.*. Mid-infrared photonic crystal cavities in silicon[J]. *Optics Express*, 2011, 19(6): 5579-5586.

#### Author Biographies:



Chang Gaiyan (1992—), female, born in Qingyang City, Gansu Province. She is a master degree candidate of the University of Chinese Academy of Sciences. She is mainly engaged in the research of ultrafast laser micro-nano machining mechanism and application. E-mail: gaiyan-chang@163.com

常改艳(1992—),女,甘肃庆阳人,中国科学院大学硕士研究生,主要从事超快激光微纳加工机理与应用研究。E-mail: gaiyanchang@163.com



Cheng Guanghua (1976—), male, born in Ankang City, Shaanxi province. He is a professor, doctoral supervisor and the visiting professor of CNRS Hubert Curie Laboratory. He is mainly engaged in the scientific research and talent training in ultrashort pulse laser technique, ultrashort laser-material interaction, femtosecond laser micro-nano machining technique and other fields. E-mail: guanghuacheng@nwpu.edu.cn

程光华(1976—),男,陕西安康人,教授,博士生导师,法国 CNRS 休伯特居里实验室,客座教授;主要从事超短脉冲激光技术,超快激光与物质相互作用、飞秒激光微纳加工技术等方面的科学研究和人才培养工作。E-mail: guanghuacheng@nwpu.edu.cn